Published in final edited form as:
Langmuir. 2013 August 20; 29(33): 10573–10578. doi:10.1021/la4022867.

Controllable In-Situ Synthesis of Magnetite Coated Silica-Core Water-Dispersible Hybrid Nanomaterials

Haiou Qu[*,†,‡], **Sheng Tong**[§], **Kejing Song**[¶], **Hui Ma**[‡], **Gang Bao**[§], **Seth Pincus**[¶], **Weilie Zhou**[‡], and **Charles O'Connor**[*,‡]

[‡] Advanced Materials Research Institute, University of New Orleans, New Orleans, 70148 United States

[§] Department of Biomedical Engineering, Georgia Institute of Technology and Emory University, Atlanta, Georgia 30332 United States

[¶] Research Institute for Children, Children's Hospital, New Orleans, LA 70118 United States

Abstract

Magnetite nanoparticle coated silica (Fe_3O_4@SiO_2) hybrid nanomaterials hold an important position in the fields of cell imaging and drug delivery. Here we report a large scale synthetic procedure that allows attachment of magnetite nanoparticles onto a silica surface *in-situ*. Many different silica nanomaterials such as Stöber silica nanospheres, mesoporous silica nanoparticles, and hollow silica nanotube have been coated with a high density layer of water-dispersible magnetite nanoparticles. The size and attachment efficiency of the magnetite nanoparticle can be well tuned by adjusting the precursor concentration and reflux time. The functionalization of Fe_3O_4@SiO_2 nanoparticles with dye molecules and biocompatible polymers impart optical imaging modality and good colloidal stability in either buffer solution or serum. The functionalized materials also exhibited strong potential as negative contrast agents in T_2 weighted magnetic resonance imaging.

Keywords

magnetite coated silica; in-situ attachment; water dispersible; cell imaging

INTRODUCTION

In the past few years, scientists have paid increasing attention to many types of nanomaterials because of their potential in the design and fabrication of the next-generation of agents for clinical purposes such as imaging, diagnosis and therapy.[1-4] Magnetic nanoparticles, especially iron oxide nanoparticles, represent a unique class of nanomaterials that have a very strong potential in biomedicine. Due to their good biocompatibility, stability in physiological environments and size dependent magnetic properties, magnetic nanoparticles play an important role in research and development of diverse techniques such as magnetic field controlled target delivery, bioseparation, and image contrast agents in

[*]**Corresponding Author**haiou.qu@fda.hhs.gov; coconnor@uno.edu.
[†]**Present Addresses** United States Food and Drug Administration/Office of Regulatory Affair/Arkansas Regional Laboratory, 3900 NCTR Road, Building 26, Jefferson, AR 72029 United States

The authors declare no competing financial interests.

Supporting Information
Additional images and characterization data. “This material is available free of charge via the Internet at http://pubs.acs.org.”

magnetic resonance imaging (MRI).[5-9] Silica nanoparticles belong to another type of important nanomaterial that also shows great potential in biomedical areas. Stöber silica has been used as a support for assembling various kinds of nanoparticles onto their surface.[10, 11] On the other hand, mesoporous silica materials with large pore size are widely investigated as a carrier for drug delivery.[12-15] Silica is also widely used as coating agent for various nanomaterials that have potential uses in biological application.[16, 17] The silica matrix effectively protects these nanomaterials from degradation and improves their biocompatibility and colloidal stability.[18, 19]

Integrating several nanostructured materials into a single agent, based on physical forces or chemical bonding can effectively combine the special properties of different materials and build multifunctional platforms that satisfy a variety of diagnostic and therapeutic purposes simultaneously.[20-22] Generally, either Stöber silica or mesoporous silica are commonly used as the starting support for the integration process, and the silica nanoparticle itself can be doped with organic dye to be made luminescent.[15, 23-25] The surface of silica nanoparticles is usually functionalized with silane in order to make reactive functional groups available (*e.g.*, amine, thiol).[26-28] Then, many types of small nanomaterials used in biological or clinical studies such as noble metal nanocrystals, quantum dots (QDs) or magnetic nanoparticles can be loaded on to the surface of silica through their affinity with amine or thiol groups. A number of research groups have reported several examples of silica based dual-functional or multifunctional nanomaterials, and these materials exhibit excellent performance in disease diagnosis and treatment.[10-12, 14, 29] Heyon et al. described the fabrication process of dye-doped mesoporous silica immobilized with multiple magnetite nanocrystals and demonstrated their strong potential in T_2 weighted MRI, fluorescence imaging and drug delivery.[12] Cheon et al. adopted similar strategy to assemble magnetite nanoparticles onto fluorescent silica nanospheres and the materials exhibited very high T_2 relaxivity (r_2).[24] The preparation methods of these types of materials usually involve multiple steps of preparation and surface functionalization of both silica and magnetic nanoparticles, which requires a considerable amount of work. It is also very important to have the ability to scale up the synthesis for the preparation of large quantities of materials. Here we report a novel *in-situ* large scale synthesis method that efficiently attaches water-dispersible magnetite nanoparticles to silica nanospheres. With this method, magnetite nanoparticles can be assembled onto any silica-based nanomaterials which may be varied in size, shape and structure. By carefully controlling the experimental condition such as chemical concentration, ratio of iron precursor with silica and reflux duration, the size of the magnetite and their attaching efficiency can be well tuned.

EXPERIMENTAL SECTION

General Information

Iron (III) acetylacetonate ($Fe(acac)_3$, 99.9%), Tetraethyl orthosilicate (TEOS, 98%), Tetraethylene glycol (TEG, 99%), Hexadecyltrimethylammonium bromide (CTAB, 99%) (3-Aminopropyl) triethoxysilane (APTES, 98%), L-arginine (98%) Fluorescein isothiocyanate (FITC, 90%), Rhodamine B isothiocyanate were purchase from Sigma-Aldrich, Methoxy PEG succinimidyl carboxymethyl ester (MPEG-SCM, MW~2000) was purchased from JenKem Technology. Bovin calf serum was purchased from Thermo Scientific. Other general chemicals and solvents such as ethanol and acetone were used as received.

Product structure and phase purity were determined by X-ray diffraction with a Philips X`pert system. Size distribution, particles morphology, crystallinity and elemental composition were studied on JEOL 2010 transmission electron microscope (TEM) with energy dispersive X-ray spectrometer (EDS) and LEO 1530VP Field Emission Scanning

Electron Microscope (FESEM). Surface composition was examined by Thermo Nicolet Nexus 670 FT-IR machine in 650-4000 cm^{-1} region and Kratos AXIS 165 X-ray Photoelectron Spectroscope. Inductively coupled plasma atomic emission spectroscopy (ICP-AES, Varian Vista-MPX) were used to calculate the net weight of iron oxide. The magnetic properties were measured by Quantum Design SQUID magnetometer (MPMS XL-7) in the temperature range 5-300K. The colloidal stability was investigated by dynamic light scattering (DLS) and zeta potential measurements (Möbius, Wyatt Technology). T_2 relaxivity was measured with a 0.47 T Bruker Minispec Analyzer MQ20 at 40°C using Carr-Purcell Meiboom-Gill spin echo method. Fluorescence images were acquired with a Zeiss LSM 510 confocal laser scanning microscope.

Synthesis of Fe_3O_4 attached silica nanostructures

Non mesoporous silica nanoparticles above 100 nm were prepared through classic Stöber method.[30] Highly monodispersed small silica spheres (<100 nm) and mesoporous silica nanospheres were prepared according to the reported method with some modifications.[31, 32] Mesoporous hollow silica nanotubes were fabricated using sol-gel method based on our previous work.[33] Fe_3O_4@SiO_2 was prepared by refluxing iron precursors, silica nanomaterials in polyalcohol for different amount of time. For 100 nm Fe_3O_4@SiO_2, for example, 100 mg of silica nanoparticles was dispersed in 1 ml of water by placing in a sonication bath for 30 min. Then 10 g of TEG and 0.177 g (0.5 mmol) of $Fe(acac)_3$ were added. The mixture was first heated to 110 °C under vacuum for 1 h to remove water, and then to 210 °C for 2h with a flow of nitrogen. The system was finally refluxed at 300 °C for 1-3 h and then cooled to room temperature. The synthesis can be scaled up by proportionally increasing the system volume and using the same chemical and silica concentration in a larger flask. The final products contained a small fraction of unbound Fe_3O_4 nanocrystals. For the purification, acetone was added to the synthesis solution and an external magnetic field was applied to precipitate the Fe_3O_4@SiO_2. The supernatant which contained free Fe_3O_4 nanocrystals was then decanted. This process was repeated five times and the product was dried under vacuum. By varying the silica form and chemical concentration, Fe_3O_4 attached silica nanostructured materials with different attaching efficiency can be prepared and the size of magnetite can also be tuned. Magnetite nanoparticles coated mesoporous silica nanosphere and hollow silica nanotubes were synthesized in a similar manner.

Surface functionalization of Fe_3O_4 attached silica nanosphere

In a 20 ml vial, 6 mg of 110 nm Fe_3O_4 attached silica sphere was fully dispersed in absolute ethanol by sonication. Then 100 μl of APTES was added and the solution was stirred overnight. After washing with ethanol for five times, APTES functionalized nanoparticles were redispersed in 4 ml of ethanol with 2 μg of FITC. The solution was stirred overnight, washed with ethanol and redispersed in 5 ml of ethanol. The amount of 40 mg of MPEG SCM was added, followed with 12 h of thorough stirring. The resulting products were washed with ethanol and dried in vacuum

Cell viability test

HeLa cells and H9 cell were seeded in triplicate with 5×10^3 cells per well. Fe_3O_4@SiO_2 of variable sizes were added. After 72 h, 30μl of MTS/PMS were added to each well and incubated for 2 h. The absorbance was read at 490 nm

In Vitro fluorescent imaging

HeLa cells were seeded in 24-well plate with coverglass at 1×10^4/well. Dye doped Fe_3O_4@SiO_2 were added to warm complete RPMI 1640 at concentration of 1, 5, 25 μg/ml and cultured in 37 °C incubator for 6 h. The culture medium was replaced with fresh RPMI

1640 containing 125 mM of LTB and incubated for 30 min. Then, cells were washed with PBS for 3 times and fixed with 2% paraformaldehyde. Cells were imaged with Zeiss LSM 510 confocal laser scanning microspcope using both oil lens and regular lens.

In Vitro MR imaging

HeLa cells were cultured with DMEM supplemented with 10% FBS. The cells were added to 6-well cell culture plates at 2×10^5 cell per well seeding density and cultured for 48 hours before use. $Fe_3O_4@SiO_2$ of variable sizes were dispersed in FBS supplemented DMEM at 100 μg/ml. The cells were cultured with the nanoparticles solutions for 4 hours. After that, the cells were washed with PBS twice and detached with trypsin-EDTA. After centrifugation, the cells were dispersed in 0.6% low-melting point agarose gel at a density of 5×10^6 cells / mL. The gel was added to a T25 flask and imaged with a Bruker 7 T small animal MRI instrument. Spin-echo sequence was used for imaging (TR/TE = 1500 ms/ 12, 24, 36, 48, 60 ms. FOV = 4×4 cm. Slice thickness = 2mm. Matrix = 256×256)

RESULTS AND DISCUSSION

Assembling iron oxide nanoparticles onto silica nanoparticles surface has been reported previously.[10, 11, 24, 28] The general idea is to prepare silica nanoparticles and magnetic nanoparticles individually and their surface moieties were functionalized so that iron oxide nanoparticles can be attached to the silica surface through reaction and form chemical bonds. Such methods are usually performed at a smaller scale and the preparation can be time consuming. We have developed a two-step procedure which produces this type of materials with higher efficiency and largely reduces the amount of time and effort. Silica nanomaterials including Stöber silica nanoparticles, mesoporous silica and hollow silica nanotubes were synthesized according to literature methods with some modifications.[30-33] A silica nanoparticle solution was mixed with iron precursor in TEG and the system was heated to reflux temperature to yield $Fe_3O_4@SiO_2$. Figure 1a is the TEM image of silica nanoparticles with average size of 109 nm prepared by the Stöber method. After the reaction (Figure 1b), numerous magnetite nanoparticles with average diameter of 8.3 nm (σ=19%) are attached onto silica nanospheres and form a thin layer of magnetite with nearly uniform distribution on the silica surface. No disassociated magnetite nanoparticles were observed either near the silica or in any other sample area. We have successfully scaled up the procedure which produced up to 5 g of product in a single batch while maintaining the same chemical concentration. Low magnification TEM and SEM images (Figure 1c&1d) suggest that all silica spheres are attached with magnetite nanoparticles throughout their surface and there is no observable variation of the attachment efficiency.

Variable sized $Fe_3O_4@SiO_2$ can be easily prepared by simply using silica nanospheres of different diameters. As shown in Figure 2a-e, silica nanoparticles with sizes from 50 nm to less than 1 micron are all covered with a layer of magnetite nanoparticles, and no detachment of Fe_3O_4 was observed in any of the product. Beside Stöber silica, the *in-situ* decoration method can be expanded to immobilize any silica nanostructure such as mesoporous silica, silica nanorod or nanotube with magnetite nanocrystals. Figure 2f-g presents the TEM images of mesoporous silica nanoparticles, hollow silica nanotubes and their downstream products after the magnetite attachment. No obvious difference was found when changing Stöber silica to mesoporous silica. Similarly, the hollow silica nanotubes are also covered with a smooth layer of magnetite nanoparticles. The mesoporous and hollow structures are of great value in target delivery because a large amount of drug molecules can be stored within the porous structure or hollow cavities. The attachment of numerous magnetite nanoparticles renders powerful magnetic properties to these silica structures, which make them promising nanomaterials for targeted drug delivery for cancer treatment.

The reaction parameters were investigated, including chemical concentration, the amount of silica and the reflux time. By maintaining constant iron precursor concentration, changing the silica nanoparticle concentration resulted in different attachment efficiencies of magnetite nanoparticles. Generally, synthesis with concentrated silica nanoparticles produced Fe_3O_4@SiO_2 with sparse attachment of magnetite nanocrystals (SI, Figure S1b&1c) whereas lower silica concentration resulted in compact attachment or even unattached magnetite nanoscrystals mixed with Fe_3O_4@SiO_2, ascribed to the less available or insufficient total surface area (SI, Figure S1d). Although the number of magnetite grains on each silica nanoparticle was directly dependent on the available surface area, the results did not suggest a strong relationship of the average size of attached magnetite with silica concentration. However, the concentration of iron precursor had an effect on both the attachment and the magnetite nanocrystal itself. It was observed that when the concentration of iron precursor was doubled, the average size of magnetite nanoparticles was increased from 8.3 nm to 10 nm (SI, Figure S2), which can be attributed to the increased amount of available iron source for particle growth, whereas diluted iron source concentration yielded silica nanospheres with less and smaller magnetite nanoparticles (SI, Figure S1e 1g). In many iron oxide nanoparticles syntheses, longer refluxing time would lead to larger particles.[34, 35] In our synthesis, refluxing at 300 °C for 3 h produced 8.3 nm magnetite nanoparticles whereas 1 h refluxing produced particles of 7.0 nm, which was consistent with reports in the literature (SI, Figure S1h). The studies of the synthetic conditions were performed on various silica nanomaterials, and similar results were observed. For example, the SEM images of 400 nm Fe_3O_4@SiO_2 synthesized under different conditions (Figure 3) clearly show that a small amount of silica would produce a compact surface coating whereas increased silica feeding would decrease the silica surface coverage.

The formation of magnetite nanoparticles on the silica surface was investigated by taking aliquots of solution at different time intervals during the preparation and then examined with TEM. It is suggested that the supersaturation of the precursor induced a rapid nucleation and the produced small nuclei tend to adsorb on the surface of silica nearby to lower their surface energy (SI, Figure S3a&b). As the reaction progressed, more and more nuclei adhered to the silica sphere and resulted in a nearly fully covered silica surface. These nuclei started to grow upon the consumption of monomers decomposed from their precursors (SI, Figure S3c&d). The Ostwald ripening process during which relatively smaller nanocrystals dissolved and then redeposited the material on adjacent bigger nanoparticles lead to a partially covered silica sphere with increased magnetite size. From TEM image (Figure S3), it is clear that nucleation was developed both on silica surface and in the synthesis medium. At higher temperatures, the surface coverage of silica was enhanced and reached to a saturation whereas nuclei concentration in reaction solution was dramatically decreased, implying the adsorption of nuclei onto the silica sphere.

To examine the stability of the magnetite on the silica surface, a small vial containing a dispersion of as-prepared Fe_3O_4@SiO_2 was immersed in a 40 kHz ultrasonic bath (Branson 1510) for several different intervals. Surprisingly, no observable change was found on the samples after 1h, 2 h and even 5 h of continuous ultrasonic treatment (SI, Figure S4), suggesting strong interaction of magnetite nanoparticles with the silica surface. The as-prepared Fe_3O_4@SiO_2 were either kept in solvents or dried under vacuum and stored at ambient condition for more than 10 months. No morphology change or dissociated magnetite nanoparticles were observed, indicating good stability and strong attachment of magnetite on silica.

The magnetic nanocrystals on silica surface were examined to be phase-pure magnetite by XRD (Figure S5). To further confirm the chemical composition of magnetite nanoparticles, the as-prepared materials were studied by XPS. The presents of two photoelectron peaks at

710.6 eV and 724.1 eV are very close to the previously reported binding energy value of core-level Fe 2p lines in magnetite (Figure S6),[36, 37] confirming the magnetite phase of the iron oxide nanoparticles on silica surface. From HRTEM image, a clear crystal lattice can be seen of a single magnetite nanoparticle on silica (Figure 1b inset), suggesting good crystallinity of the nanoparticles. The surface composition of Fe_3O_4@SiO_2 was examined in FT-IR (Figure 4). The emerging peaks in 2800 cm^{-1} to 3000 cm^{-1} section and a few more bands around 1460 cm^{-1} in Fe_3O_4@SiO_2, which were absent in pure silica nanospheres, arise from the C-H bond stretching from methylene groups, indicating the presence of TEG molecules.[38] To further confirm the presents of TEG as capping ligand on magnetite, we examined the spectrum of magnetite nanoparticles prepared in TEG (no silica nanoparticles were added). As clearly shown in the figure, the spectrum of TEG coated magnetite nanoparticles shared many similar bands with the spectrum of Fe_3O_4@SiO_2.

Magnetic measurements showed that all Fe_3O_4@SiO_2 were superparamagnetic at room temperature with different saturation magnetizations (M_s) that were closely related to the synthesis conditions (SI. Figure S7). Smaller Fe_3O_4@SiO_2 exhibited relatively higher M_s because of the decreased size of non magnetic silica core which led to higher iron content of each particle. Other synthesis conditions that would affect the attaching efficiency or the size of magnetite can also cause variation of the saturation magnetization values.

Silica nanostructures with magnetite nanoparticles attached on their surface have been demonstrated to possess good capacities in several biological applications such as drug delivery and cell imaging.[39] We applied two simple tests to study the potentials of Fe_3O_4@SiO_2 prepared by our method for cell imaging applications. In order to fabricate dual-functional or multifunctional probes for different imaging mode, organic dyes or QDs are commonly incorporated. Here, fluorescein isothiocyanate (FITC) was chosen as a dye to dope the particles. The functionalized particles are stable in buffer solution and serum (SI, Figure S8). Under a confocal laser scanning microscope (CLSM), dye doped Fe_3O_4@SiO_2 exhibited a bright green color fluorescence. The merged images suggest that dye molecules were successfully introduced to Fe_3O_4@SiO_2. The cellular uptake of dye doped Fe_3O_4@SiO_2 was also studied by CLSM after 6 h incubation of HeLa cell with the materials (Figure 4). A green fluorescent color was observed in the intracellular region. Under sectioning mode (SI, Figure S9), images of a single cell at different depths of focus were acquired from the bottom to the top of the cell. It is clearly demonstrated that dye doped Fe_3O_4@SiO_2 nanomaterials were internalized by the HeLa cells rather than adsorbed on cell membranes. The cytotoxicity of the Fe_3O_4@SiO_2 of different sizes was tested with both human lymphoblastoma cell line (H9 cell) and HeLa cell line. After 72 h of exposure to Fe_3O_4@SiO_2, no significant cytotoxicity was observed for particle concentration up to 1 mg/ml (SI, Figure S10).

Many previous reports have suggested that assembled magnetic iron oxide nanoparticles on silica structures possess a strong potential in enhancing the contrast of MR images.[12, 24] Fe_3O_4@SiO_2 of 55, 110 and 130 nm were chosen to test their performance as contrast agents in T_2-weighted MRI (Figure 6). From solution studies, all of the three samples showed a remarkable MR T_2 contrast in a concentration dependent manner. The linear relationship of the T_2 relaxation rate to Fe concentration was plotted and their r_2 are 365, 144 and 120 mM^{-1} s^{-1} respectively, which are close or higher than many other similar probes reported in the literature. For *in vitro* imaging studies, Fe_3O_4@SiO_2 of different sizes were incubated with human cervical carcinoma HeLa cell lines and T_2 weighted images were acquired. It is clear that after 4 h of incubation, cells treated with Fe_3O_4@SiO_2 presented darken images, suggesting the potentials of these nanoparticles as MRI probes.

CONCLUSION

We have demonstrated a large scale synthesis method to prepare silica nanostructured materials with attached water-dispersible magnetite nanoparticles with controllable attachment efficiency. The sizes of the attached magnetite nanoparticles can be tuned by adjusting the concentration of iron precursors or reflux time. This strategy simplifies traditional fabrication processes and allows production of various nanostructured materials to serve different application purposes. The magnetite nanoparticles exhibited excellent stability on the silica surface, and the materials possessed good colloidal stability in buffer solution or biological matrices. *In vitro* studies have shown good performance of $Fe_3O_4@SiO_2$ in MRI with shortening of the T_2 relaxivity, and dye doped $Fe_3O_4@SiO_2$ also presented good fluorescent imaging properties. Such materials have great potential as dual-functional probes in cell imaging, and the synthesis method will also benefit the preparation of many other types of nanofunctional materials.

Supplementary Material

Refer to Web version on PubMed Central for supplementary material.

Acknowledgments

This work was financially supported by a research grant from Louisiana Board of Regents contract no. LEQSF(2007-12)-ENH-PKSFI-PRS-04 and by the National Heart Lung and Blood Institute of the NIH as a Program of Excellence in Nanotechnology Award (HHSN268201000043C to GB).

REFERENCES

1. Hou Y, Qiao R, Fang F, Wang X, Dong C, Liu K, Liu C, Liu Z, Lei H, Wang F, Gao M. NaGdF4 Nanoparticle-Based Molecular Probes for Magnetic Resonance Imaging of Intraperitoneal Tumor Xenografts in Vivo. ACS Nano. 2012; 7(1):330–338. [PubMed: 23199030]
2. Sapsford K, Pons T, Medintz I, Mattoussi H. Biosensing with Luminescent Semiconductor Quantum Dots. Sensors. 2006; 6(8):925–953.
3. Kang X, Yang D, Ma P. a. Dai Y, Shang M, Geng D, Cheng Z, Lin J. Fabrication of Hollow and Porous Structured GdVO4:Dy3+ Nanospheres as Anticancer Drug Carrier and MRI Contrast Agent. Langmuir. 2013; 29(4):1286–1294. [PubMed: 23281806]
4. Cheng Y, Qu H, Ma M, Xu Z, Xu P, Fang Y, Xu T. Polyamidoamine (PAMAM) dendrimers as biocompatible carriers of quinolone antimicrobials: An in vitro study. Eur. J. Med. Chem. 2007; 42(7):1032–1038.
5. Tong S, Ren B, Zheng Z, Shen H, Bao G. Tiny Grains Give Huge Gains: Nanocrystal-Based Signal Amplification for Biomolecule Detection. ACS Nano. 2013
6. Qu H, Ma H, Riviere A, Zhou W, O'Connor CJ. One pot synthesis in polyamines for preparation of water-soluble magnetite nanoparticles with amine surface reactivity. J. Mater. Chem. 2012; 22(8): 3311–3313.
7. Lu X, Niu M, Qiao R, Gao M. Superdispersible PVP Coated Fe3O4 Nanocrystals Prepared by a “One-Pot” Reaction†. J. Phys. Chem. B. 2008; 112(46):14390–14394. [PubMed: 18671367]
8. Sanson C, Diou O, Thévenot J, Ibarboure E, Soum A, Brûlet A, Miraux S, Thiaudière E, Tan S, Brisson A, Dupuis V, Sandre O, Lecommandoux S. b. Doxorubicin Loaded Magnetic Polymersomes: Theranostic Nanocarriers for MR Imaging and Magneto-Chemotherapy. ACS Nano. 2011; 5(2):1122–1140. [PubMed: 21218795]
9. Hultman KL, Raffo AJ, Grzenda AL, Harris PE, Brown TR, O'Brien S. Magnetic Resonance Imaging of Major Histocompatibility Class II Expression in the Renal Medulla Using Immunotargeted Superparamagnetic Iron Oxide Nanoparticles. ACS Nano. 2008; 2(3):477–484. [PubMed: 19206573]

10. Kim J, Lee JE, Lee J, Jang Y, Kim SW, An K, Yu JH, Hyeon T. Generalized Fabrication of Multifunctional Nanoparticle Assemblies on Silica Spheres. Angew. Chem. Int. Ed. 2006; 45(29): 4789–4793.
11. Stoeva SI, Huo F, Lee JS, Mirkin CA. Three-Layer Composite Magnetic Nanoparticle Probes for DNA. J. Am. Chem. Soc. 2005; 127(44):15362–15363. [PubMed: 16262387]
12. Lee JE, Lee N, Kim H, Kim J, Choi SH, Kim JH, Kim T, Song IC, Park SP, Moon WK, Hyeon T. Uniform Mesoporous Dye-Doped Silica Nanoparticles Decorated with Multiple Magnetite Nanocrystals for Simultaneous Enhanced Magnetic Resonance Imaging, Fluorescence Imaging, and Drug Delivery. J. Am. Chem. Soc. 2009; 132(2):552–557. [PubMed: 20017538]
13. Yu Q, Wang P, Hu S, Hui J, Zhuang J, Wang X. Hydrothermal Synthesis of Hollow Silica Spheres under Acidic Conditions. Langmuir. 2011; 27(11):7185–7191. [PubMed: 21553827]
14. Huang S, Fan Y, Cheng Z, Kong D, Yang P, Quan Z, Zhang C, Lin J. Magnetic Mesoporous Silica Spheres for Drug Targeting and Controlled Release. J. Phys. Chem. C. 2009; 113(5):1775–1784.
15. Wang T, Zhang L, Su Z, Wang C, Liao Y, Fu Q. Multifunctional Hollow Mesoporous Silica Nanocages for Cancer Cell Detection and the Combined Chemotherapy and Photodynamic Therapy. ACS Appl. Mater. Inter. 2011; 3(7):2479–2486.
16. Jing L, Yang C, Qiao R, Niu M, Du M, Wang D, Gao M. Highly Fluorescent CdTe@SiO2 Particles Prepared via Reverse Microemulsion Method. Chem. Mater. 2009; 22(2):420–427.
17. Dai Y, Ma P. a. Cheng Z, Kang X, Zhang X, Hou Z, Li C, Yang D, Zhai X, Lin J. Up-Conversion Cell Imaging and pH Induced Thermally Controlled Drug Release from NaYF4:Yb3+/Er3+@Hydrogel Core–Shell Hybrid Microspheres. ACS Nano. 2012; 6(4):3327–3338. [PubMed: 22435911]
18. Jana NR, Earhart C, Ying JY. Synthesis of Water-Soluble and Functionalized Nanoparticles by Silica Coating. Chem. Mater. 2007; 19(21):5074–5082.
19. Deng Y, Qi D, Deng C, Zhang X, Zhao D. Superparamagnetic High-Magnetization Microspheres with an Fe3O4@SiO2 Core and Perpendicularly Aligned Mesoporous SiO2 Shell for Removal of Microcystins. J. Am. Chem. Soc. 2007; 130(1):28–29. [PubMed: 18076180]
20. Insin N, Tracy JB, Lee H, Zimmer JP, Westervelt RM, Bawendi MG. Incorporation of Iron Oxide Nanoparticles and Quantum Dots into Silica Microspheres. ACS Nano. 2008; 2(2):197–202. [PubMed: 19206619]
21. Qu H, Ma H, Zhou W, O'Connor CJ. In situ surface functionalization of magnetic nanoparticles with hydrophilic natural amino acids. Inorg. Chim. Acta. 2012; 389(0):60–65.
22. Nasongkla N, Bey E, Ren J, Ai H, Khemtong C, Guthi JS, Chin SF, Sherry AD, Boothman DA, Gao J. Multifunctional Polymeric Micelles as Cancer-Targeted, MRI Ultrasensitive Drug Delivery Systems. Nano Lett. 2006; 6(11):2427–2430. [PubMed: 17090068]
23. Fan Y, Yang P, Huang S, Jiang J, Lian H, Lin J. Luminescent and Mesoporous Europium-Doped Bioactive Glasses (MBG) as a Drug Carrier. J. Phys. Chem. C. 2009; 113(18):7826–7830.
24. Lee J-H, Jun Y.-w. Yeon S-I, Shin J-S, Cheon J. Dual-Mode Nanoparticle Probes for High-Performance Magnetic Resonance and Fluorescence Imaging of Neuroblastoma. Angew. Chem. Int. Ed. 2006; 45(48):8160–8162.
25. Kang X, Cheng Z, Li C, Yang D, Shang M, Ma P. a. Li G, Liu N, Lin J. Core–Shell Structured Up-Conversion Luminescent and Mesoporous NaYF4:Yb3+/Er3+@nSiO2@mSiO2 Nanospheres as Carriers for Drug Delivery. J. Phys. Chem. C. 2011; 115(32):15801–15811.
26. Roy I, Ohulchanskyy TY, Pudavar HE, Bergey EJ, Oseroff AR, Morgan J, Dougherty TJ, Prasad PN. Ceramic-Based Nanoparticles Entrapping Water-Insoluble Photosensitizing Anticancer Drugs: A Novel Drug–Carrier System for Photodynamic Therapy. J. Am. Chem. Soc. 2003; 125(26): 7860–7865. [PubMed: 12823004]
27. Huh S, Wiench JW, Yoo J-C, Pruski M, Lin VSY. Organic Functionalization and Morphology Control of Mesoporous Silicas via a Co-Condensation Synthesis Method. Chem. Mater. 2003; 15(22):4247–4256.
28. Valenstein JS, Kandel K, Melcher F, Slowing II, Lin VSY, Trewyn BG. Functional Mesoporous Silica Nanoparticles for the Selective Sequestration of Free Fatty Acids from Microalgal Oil. ACS Appl. Mater. Inter. 2012; 4(2):1003–1009.

29. Chan Y, Zimmer JP, Stroh M, Steckel JS, Jain RK, Bawendi MG. Incorporation of Luminescent Nanocrystals into Monodisperse Core–Shell Silica Microspheres. Adv. Mater. 2004; 16(23-24): 2092–2097.
30. Bogush GH, Tracy MA, Zukoski Iv CF. Preparation of monodisperse silica particles: Control of size and mass fraction. J. Non-Cryst. Solids. 1988; 104(1):95–106.
31. Hartlen KD, Athanasopoulos APT, Kitaev V. Facile Preparation of Highly Monodisperse Small Silica Spheres (15 to >200 nm) Suitable for Colloidal Templating and Formation of Ordered Arrays. Langmuir. 2008; 24(5):1714–1720. [PubMed: 18225928]
32. He Q, Cui X, Cui F, Guo L, Shi J. Size-controlled synthesis of monodispersed mesoporous silica nano-spheres under a neutral condition. Microporous Mesoporous Mater. 2009; 117(3):609–616.
33. Ma H, Tarr J, DeCoster MA, McNamara J, Caruntu D, Chen JF, O'Connor CJ, Zhou WL. Synthesis of magnetic porous hollow silica nanotubes for drug delivery. J. Appl. Phys. 2009; 105(7):07B309–3.
34. Li Z, Chen H, Bao H, Gao M. One-Pot Reaction to Synthesize Water-Soluble Magnetite Nanocrystals. Chem. Mater. 2004; 16(8):1391–1393.
35. Li Z, Sun Q, Gao M. Preparation of Water-Soluble Magnetite Nanocrystals from Hydrated Ferric Salts in 2-Pyrrolidone: Mechanism Leading to Fe3O4. Angew. Chem. Int. Ed. 2005; 44(1):123–126.
36. Gaur S, Johansson S, Mohammad F, Kumar CSSR, Spivey JJ. Catalytic Activity of Titania-Supported Core–Shell Fe3O4@Au Nano-Catalysts for CO Oxidation. J. Phys. Chem. C. 2012; 116(42):22319–22326.
37. Teng X, Black D, Watkins NJ, Gao Y, Yang H. Platinum-Maghemite Core–Shell Nanoparticles Using a Sequential Synthesis. Nano Lett. 2003; 3(2):261–264.
38. Qu H, Caruntu D, Liu H, O'Connor CJ. Water-Dispersible Iron Oxide Magnetic Nanoparticles with Versatile Surface Functionalities. Langmuir. 2011; 27(6):2271–2278.
39. Lin Y-S, Wu S-H, Hung Y, Chou Y-H, Chang C, Lin M-L, Tsai C-P, Mou C-Y. Multifunctional Composite Nanoparticles: Magnetic, Luminescent, and Mesoporous. Chem. Mater. 2006; 18(22): 5170–5172.

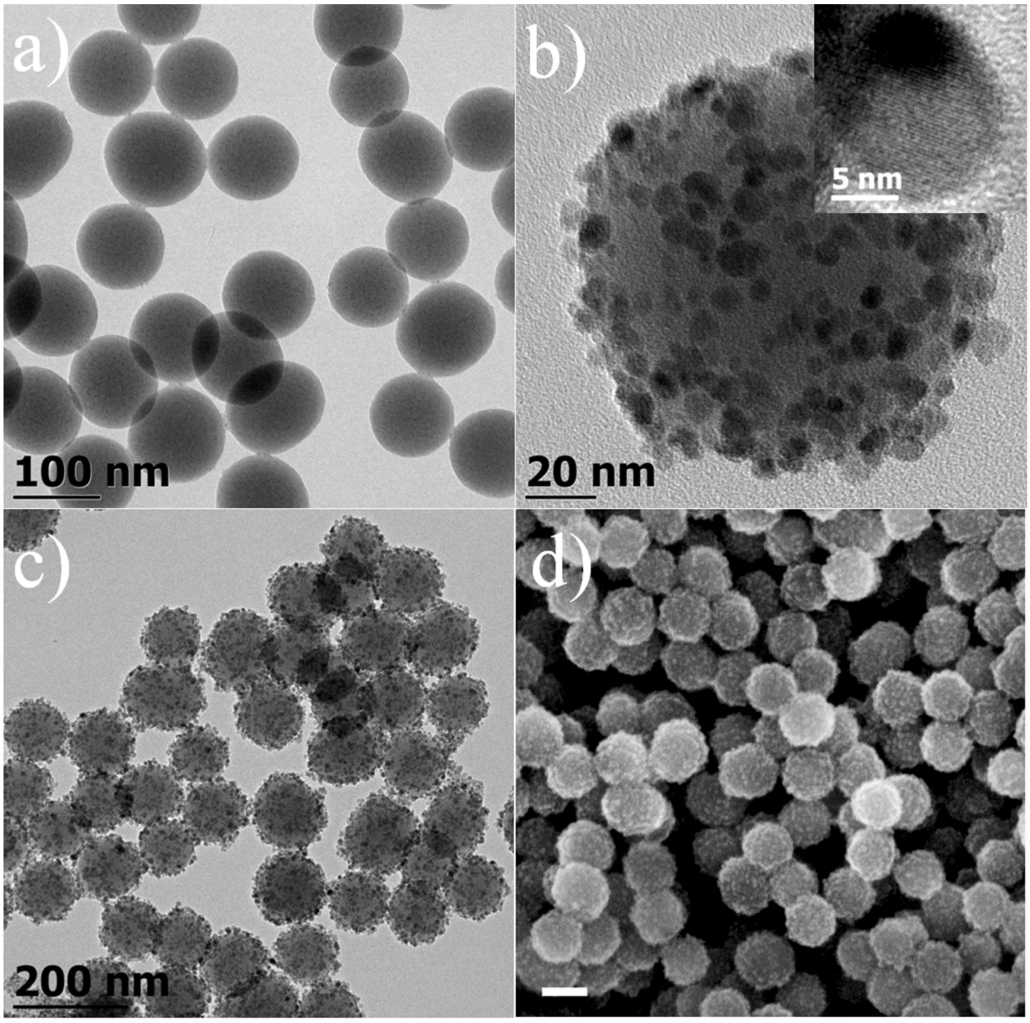

Figure 1.
TEM images of (a) 109 nm Stöber silica nanospheres, (b) a single 109 nm silica nanosphere attached with 8.3 nm magnetite nanocrystals (inset: high resolution TEM image of an attached magnetite nanocrystal). (c) lower magnification of large areas of magnetite attached silica nanosphere. (d) SEM image of 109 nm Fe_3O_4@SiO_2 (scale bar=100 nm).

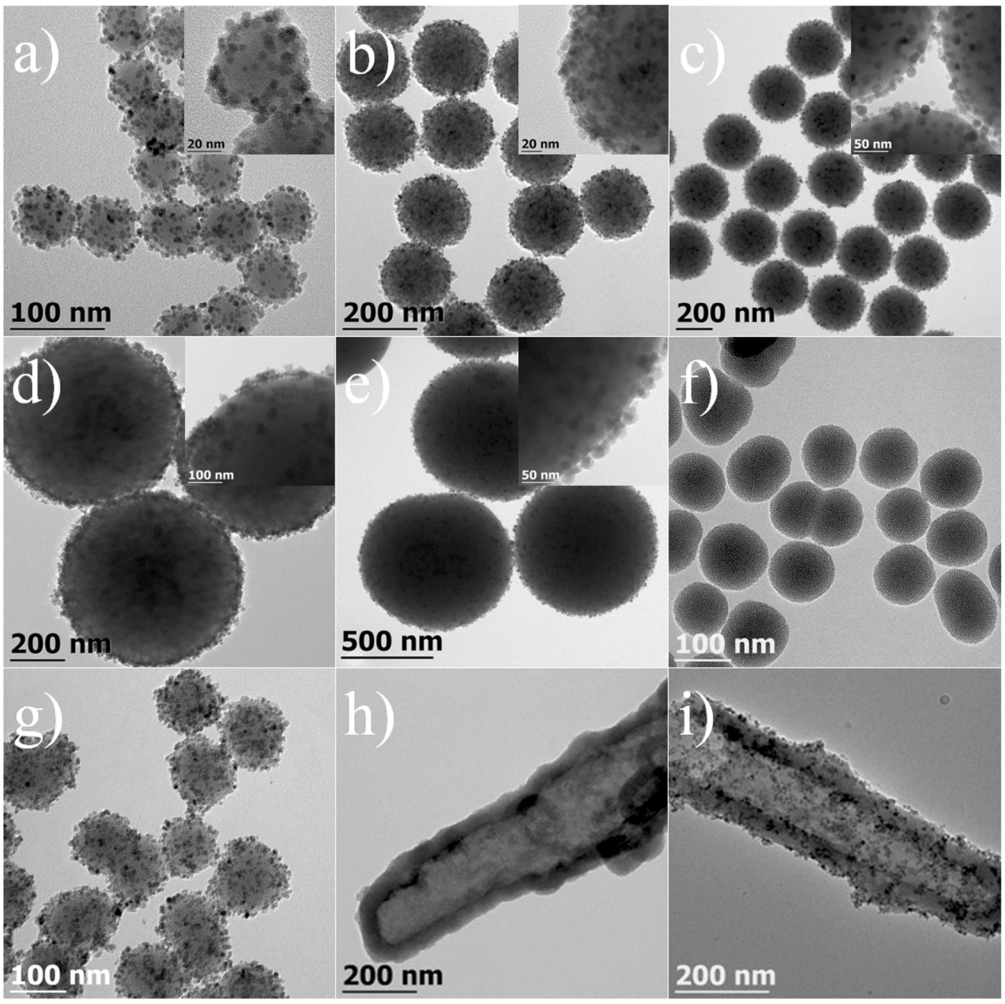

Figure 2.

TEM images of Fe_3O_4@SiO_2 (a-e, g, i) and silica nanomaterials (f, h). (a) 55 nm, (b) 185 nm, (c) 310 nm (d) 650 nm, (e) 930 nm. (f, g) 103 nm mesoporous silica nanoparticles before and after the attachment of magnetite nanocrystals. (h, i) hollow silica nanotube before and after the attachment of magnetite nanocrystals; the insets are the higher magnification images of a single Fe_3O_4@SiO_2

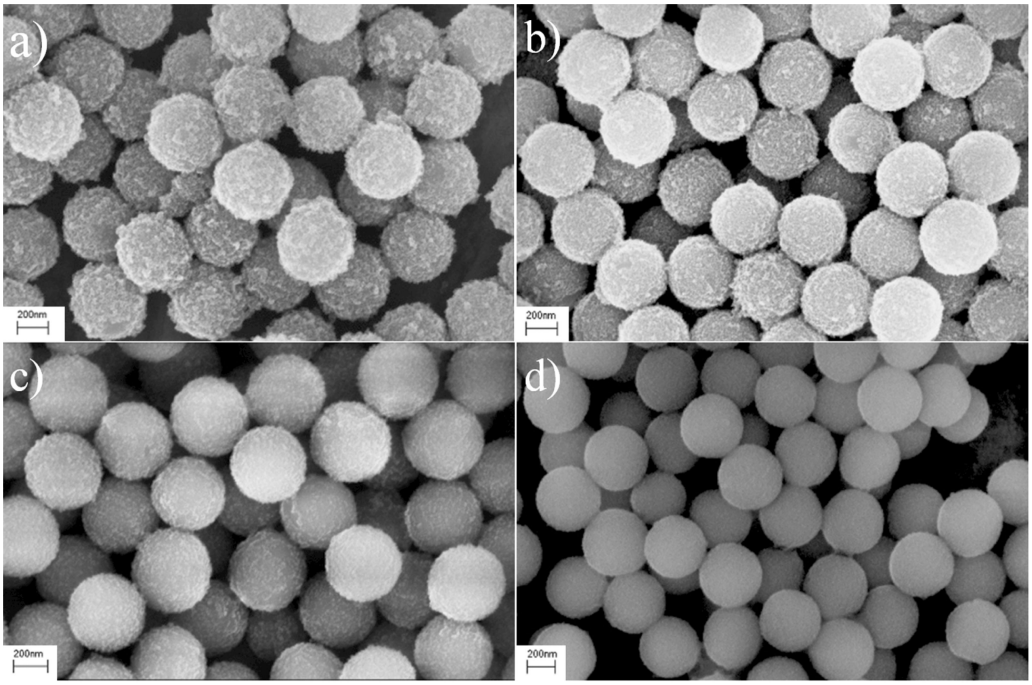

Figure 3.
SEM images of 400 nm Fe_3O_4@SiO_2 prepared under different iron precursor to silica weight ratio. (a) 1.77:1, (b) 1.77:2, (c) 1.77:4, (d) 1.77:6.

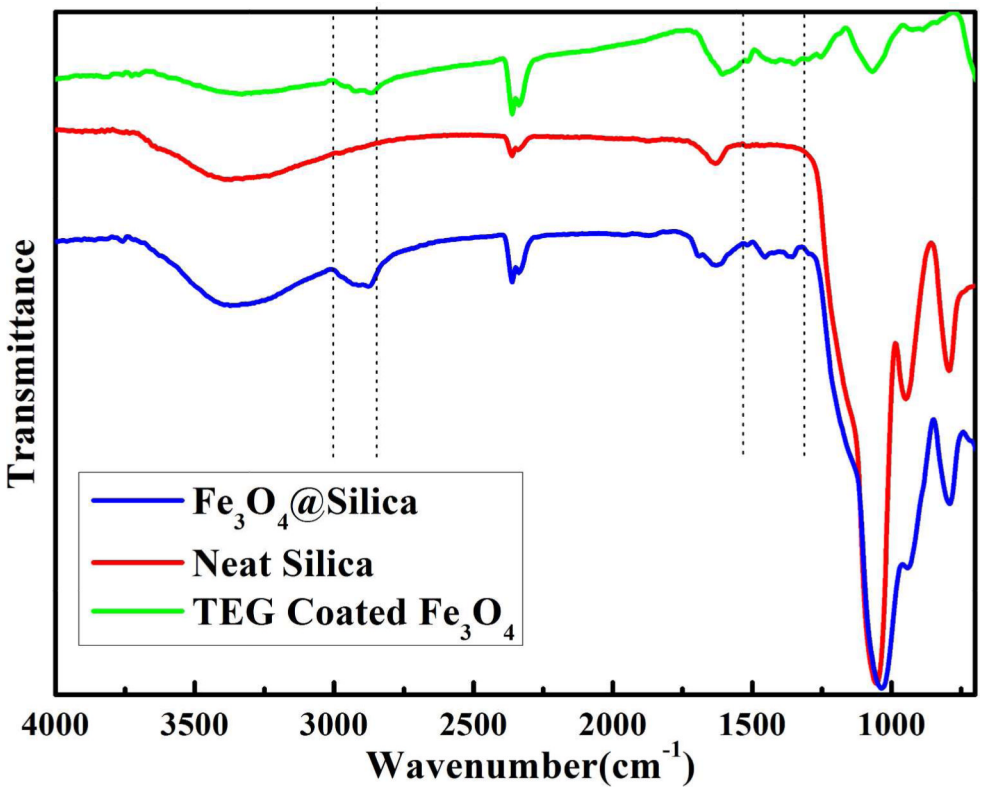

Figure 4.
(a) FT-IR spectra of neat silica, TEG coated iron oxide nanoparticles and magnetite attached silica nanocomposite.

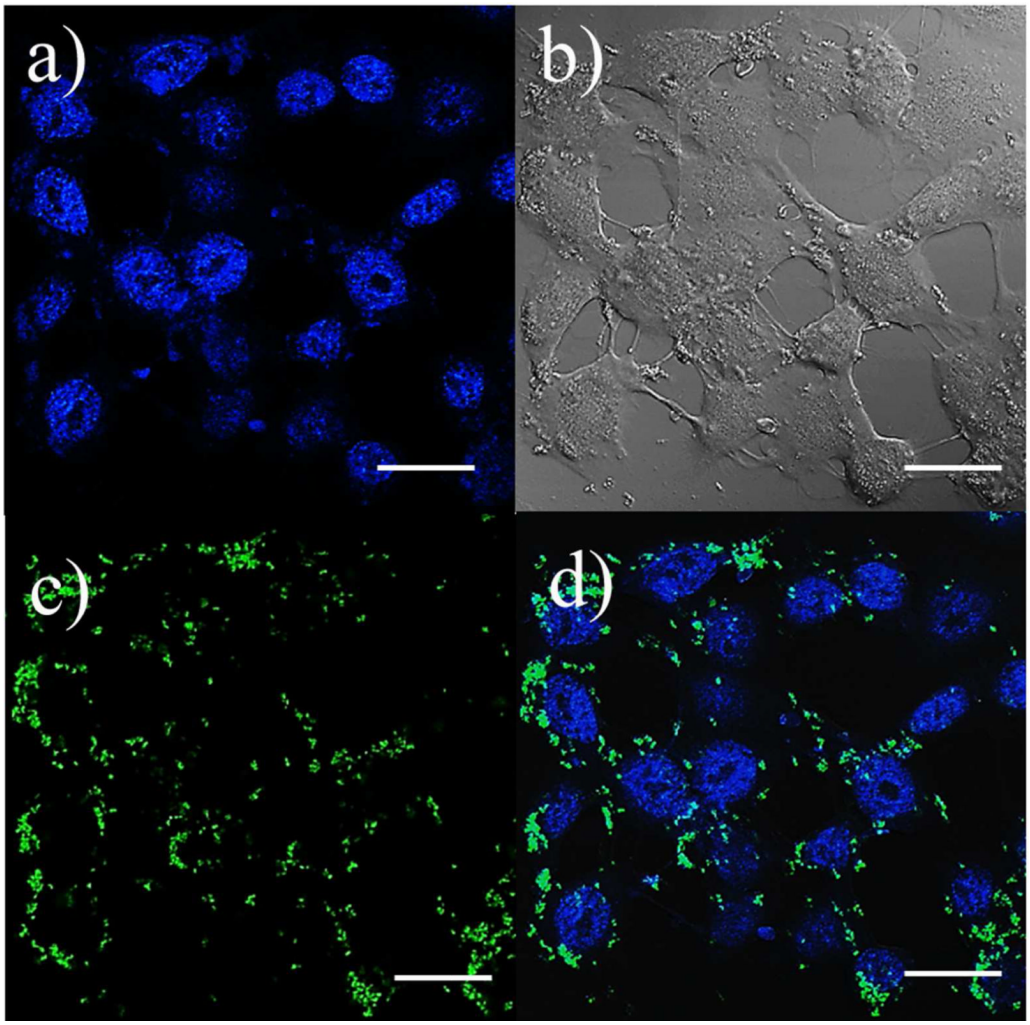

Figure 5.
Confocal laser scanning microscopic images of Hela cells incubated with 55 nm Fe_3O_4@SiO_2 at 37 °C for 6 h. (a) image of treated Hela cell with stained nuclei, (b) differential interference contrast (DIC) image. (c) green color fluorescent spots in cytoplasm region. (d) merged image of (a), (b) and (c). (scale bar=20 μm)

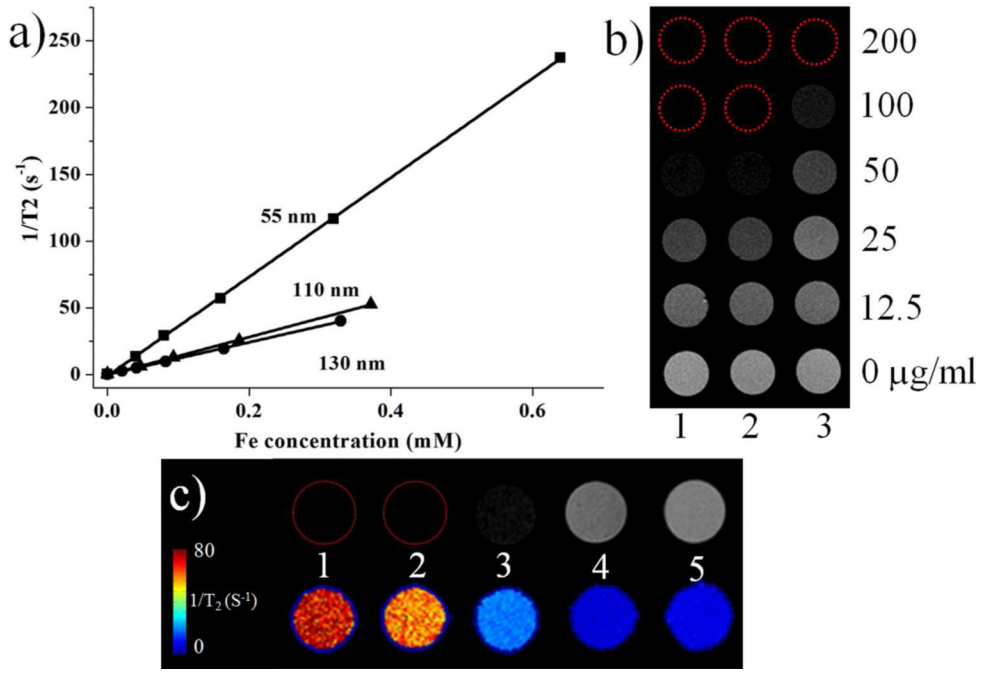

Figure 6.

(a) Transverse relaxation rates ($1/T_2$, s^{-1}) of three different sizes of $Fe_3O_4@SiO_2$ as a function of iron concentration (mM). (b) their T_2 weighted MR images (1. 55nm, 2. 110 nm, 3. 130 nm $Fe_3O_4@SiO_2$). (c) MR images of Hela cells after 4 h of incubation with 100 μg/mL of $Fe_3O_4@SiO_2$ and calculated T_2 effect based on MRI images (1. 55nm, 2. 110 nm, 3. 130 nm of $Fe_3O_4@SiO_2$, 4. control, 5 agarose). Cells were dispersed in 0.6% low melting point agarose gel at a density of 5×10^6 cells/mL.